Effects of hot isostatic pressing and heat treatments on structural and corrosion properties of direct metal laser sintered parts

Mustafa Safa Yılmaz, Gökhan Özer and Zafer Çağatay Öter
Department of Aluminum Test Training and Research Center (ALUTEAM), Fatih Sultan Mehmet Vakif University, Istanbul, Turkey, and
Onur Ertuğrul
Department of Materials Science and Engineering, Izmir Katip Celebi University, Izmir, Turkey

Abstract

Purpose – This paper aims to investigate the effects of various heat treatments on microstructure, hardness, porosity and corrosion properties of the parts.

Design/methodology/approach – Hot isostatic pressing (HIP) process, various heat treatments and their combinations were applied to the AlSi10Mg parts produced by direct laser metal sintering (DMLS).

Findings – It has been found that the HIP process, which is a post-processing process, reduces the amount of porosity in DMLS-AlSi10Mg material, thus improves corrosion resistance significantly.

Originality/value – In this study, the HIP process and subsequent T6 heat treatments were applied to AlSi10Mg parts produced by the DMLS technique. The study aims to increase the corrosion resistance of AlSi10Mg parts by reducing porosity with the HIP process and by altering the microstructure with the T6 process.

Keywords Hot isostatic pressing (HIP), Direct metal laser sintering (DMLS), Heat treatment, AlSi10Mg, Additive manufacturing (AM), Corrosion resistance

Paper type Research paper

1. Introduction

Interest in metal-based additive manufacturing (AM) systems has been increasing in recent years. They can provide quick and easy solutions to the demands of defense, aerospace and medical industries. Capabilities of these technologies offer design freedom without any loss in material (Ti, Ni, Co, Al, etc.) properties (Herzog *et al.*, 2016; Olakanmi *et al.*, 2015; Girelli *et al.*, 2019a; Wang *et al.*, 2016; Vrancken *et al.*, 2012; Sing *et al.*, 2016; Ni *et al.*, 2019). It is possible to produce many complex shaped parts in various industries with AM systems, even parts that cannot be produced by traditional methods such as "dies with built-in channels" (Kempen *et al.*, 2012; Iturrioz *et al.*, 2018).

The most common aluminum alloy used in metal AM technology is AlSi10Mg, which is the equivalent of the A360 casting alloy. This alloy has good mechanical properties, low thermal expansion coefficient, and superior corrosion resistance (Girelli *et al.*, 2019c; Delahaye *et al.*, 2019; Read *et al.*, 2015). Due to the nature of the AM process, high cooling rates in production result in eutectic compounds that are fine-grained and rich in silicon, resulting in higher tensile strength, higher hardness and higher ductility compared to conventional casting products (Kempen *et al.*, 2012; Iturrioz *et al.*, 2018; Girelli *et al.*, 2019c; Delahaye *et al.*, 2019; Read *et al.*, 2015). Also, there are many parameters that affect the properties of the material such as volume distance and scanning speed. Those parameters play an important role in material porosity and directly affect it is mechanical (fatigue, abrasion, creep) properties (Girelli *et al.*, 2019a; Krishnan *et al.*, 2013; Wang *et al.*, 2018).

The use of heat treatment to improve the mechanical properties of materials is also essential for AM, as heat treatment has an enormous impact on the microstructure and final performance (Girelli *et al.*, 2019a; Girelli *et al.*, 2019c; Wang *et al.*, 2018; Salman *et al.*, 2019). Among these, T6-like heat treatments are the most widely researched processes for AlSi10Mg alloys (Girelli *et al.*, 2019b). Studies have shown that the aging time of T6 treatment directly affects the hardness of the material (Zhou *et al.*, 2018), increases ductility (Wang *et al.*, 2018; Aboulkhair *et al.*, 2016), promotes the growth of Si particles with increasing temperature (Li *et al.*, 2016) and affects the anisotropy behaviour (Girelli *et al.*, 2019c). In addition to T6-like treatments, the hot isostatic pressing (HIP) process, which is a very effective secondary process that reduces the amount of porosity in the parts, is frequently applied to AM samples (Girelli *et al.*, 2019a; Schneller *et al.*, 2019). Although the HIP is a high-cost process, it provides a significant increase

The current issue and full text archive of this journal is available on Emerald Insight at: **https://www.emerald.com/insight/1355-2546.htm**

Rapid Prototyping Journal
 [ISSN 1355-2546]
[DOI 10.1108/RPJ-10-2020-0245]

Received 13 October 2020
Revised 9 February 2021
Accepted 2 April 2021

in ductility and corrosion properties and fatigue strength (Ran *et al.*, 2006; Lee *et al.*, 2003; Ceschini *et al.*, 2008), all of which are very critical properties for aluminum parts.

As aluminum alloys are frequently used in aerospace and automotive industries, it is not enough to provide strength only as mechanical strength. At the same time, it must have high corrosion resistance. Recently, the effects of thermal post-processing (HIP, heat treatments, etc.) on AM parts have been studied. The effects of HIP treatment on reduction of internal porosity, fatigue strength and mechanical properties of AM parts were investigated (Maamoun *et al.*, 2018). Besides, in the literature, there are studies on the corrosion properties of AM parts (Ti, steel, etc.) treated with HIP as a secondary process. Still, there is no study on the effects of the HIP treatment on the corrosion behaviour of AlSi10Mg products. The effects of AlSi10Mg alloys produced with AM on corrosion behaviour have been previously investigated. These studies are generally about the investigation of the effects of heat treatment conditions on corrosion (Gu *et al.*, 2019; Cabrini *et al.*, 2018; Rafieazada *et al.*, 2019). In addition, the effects of different chemical solutions were also examined. In this study, it was also reported that open porosity affects corrosion resistance by creating preferred corrosion starting zones (Cabrini *et al.*, 2016c). In another study, the effects of different surface finishing processes on corrosion were investigated (Cabrini *et al.*, 2016b).

The aim of the study is to increase the corrosion resistance of AlSi10Mg parts by reducing porosity with the HIP process and by altering the microstructure with the T6 process.

2. Experimental procedures

2.1 Material and production

Spherical gas atomized AlSi10Mg powder with an average particle size of 40 μm supplied by EOS GmbH was used for production of the parts. The chemical composition of the powder used is given in Table 1.

In the production stage, cylindrical test samples were produced by the DMLS method, using the EOS M 290 metal AM system. All samples were produced horizontally. DMLS production parameters are given in Table 2.

Energy density is calculated according to the equation as follows:

$$E = \frac{\mathrm{P}}{\mathrm{v.h.t}} \quad (1)$$

in which E indicates the energy density (J/mm^3); P, laser power (W); V, scan speed (mm/s); h is the hatch distance (mm) and t shows the layer thickness (mm), respectively.

Table 1 Chemical composition of AlSi10Mg powder (Wt.%)

Si	Fe	Cu	Mn	Mg	Ni	Zn	Pb	Ti	Al
9.8	0.14	0.02	<0.01	0.36	0.01	<0.01	<0.01	0.01	Rest

2.2 HIP and heat treatment conditions

Heat treatments were carried out according to the EOS datasheet (EOS, 2009). Post-production stress-relieving (SR) heat treatment was applied to all samples at 300°C for 2 h. Solution treatment (solutionizing) was applied at 540°C for 2 h. Samples were then quenched in 80°C water. Aging was carried out at 180°C for various durations. All heat treatments were carried out under ambient atmosphere in Nabertherm N 41/H furnace. Sample coding and process design are given in Table 3. The HIP process was performed under argon atmosphere and 100 MPa pressure at 500°C for 75 min. HIP furnace (AIP press HP 630 model, USA) use graphite heating elements (Figure 1). The average heating rate for HIPing was 12°C/min, and the cooling rate was 50°C/min. The whole process cycle lasted approximately 3 h.

2.3 Microstructural characterization

The samples were prepared according to the standard metallographic preparation procedure by cutting, polishing and then etching with Keller's Solution (95 mL of distilled water, 2.5 mL of HNO_3, 1 mL of HF and 1.5 mL of HCl). Optical micrographs were taken using Zeiss Axio Lab. A1 light metal microscope. Scanning electron microscope scanning electron microscope (SEM) (Hitachi SU3500 T2) and energy dispersive x-ray spectrometer (Oxford EXACT energy-dispersive X-ray spectroscopy) were used for further investigation. Quantitative analysis of the micrographs was performed (approximately 40 measurements) using the ImageJ software.

Approximately 60 pieces of silicon particles were measured from SEM micrographs and a table was created from the average values of them.

2.4 Mechanical tests

Brinell hardness (HB) measurements of the samples were conducted using an EmcoTest Duravision hardness tester by applying 62.5 kgf load using a 2.5 mm steel ball intender. Mean hardness values were calculated using five measurements conducted on a single sample.

2.5 Corrosion characterization

2.5.1 Electrochemical corrosion tests

The electrochemical corrosion behaviour of the samples was characterized by potentiodynamic polarization tests according to ASTM G5-14 standard using IVIUM/Vertex-CompactStat model potentiostat. Tests were carried out in 3.5% wt. NaCl solution with a scanning rate of 0.5 mV/s. Before potentiodynamic polarization tests, the samples were polished, cleaned with acetone, and dried with hot air. The corrosion test cell consisted of the reference electrode-RE (Ag/AgCl), working electrode-WE (MS1 samples), and a counter electrode-CE (platinum). Surface areas of the working electrode and the counter electrode were determined as 1 cm^2. At the beginning of a potentiodynamic test, open-circuit potential was measured after 40 min. Corrosion potential (E_{corr}), corrosion progression rate (i_{corr}), polarization resistance (R_p) and

Table 2 DMLS parameters

Laser power (W)	Scan speed (mm/s)	Hatch distance (mm)	Layer thickness (μm)	Energy density (J/mm^3)
370	1,300	0.19	30	49.93

Table 3 Sample coding and corresponding thermal processes

Sample code	Process
H0	DMLS + SR*
H1	DMLS + SR + HIP
H2	DMLS + SR + HIP + solutionizing** + 4-h aged***
H3	DMLS + SR+ HIP + solutionizing + 12-h aged
T6	DMLS + SR + solutionizing + 4-h aged

Notes: *SR heat treatment: 300°C/2h + air cooling; **solutionizing heat treatment: 540°C/2h + 80°C water quench; ***aging temperature: 180°C

Figure 1 Graphite heating setup with a set of samples

corrosion rate (mm/year) were obtained by the Tafel extrapolation method using IviumSoft software according to ASTM G3-14.

2.5.2 Intergranular corrosion tests

IGC tests were carried out according to BS EN ISO 11846:2008 standard-method B. Before IGC testing, samples were degreased with acetone, immersed for 2 min in NaOH solution [5% (m/m)] at a temperature of 60°C, washed in running water, immersed for 2 min in concentrated nitric acid for desmutting, and rinsed in running water and then in distilled water and dried. After that, samples were immersed for 24 h in a solution containing 30 g/l NaCl and 10 mL ± 1mL of concentrated HCl at room temperature. After the tests, the samples were rinsed in running water and distilled water and dried. The corrosion products on the sample surfaces were then cleaned, and the weight losses of the samples were calculated using a precision-scale.

Based on the weight loss calculated as the difference between the initial weight of the sample before immersion and its weight after the removal of corrosion product, the corrosion rates (mm/year) of the samples were determined using the formula below:

$$R_{corr.} = 87.6 \text{ x } \frac{W}{D.A.T} \quad (2)$$

In this formula, $R_{corr.}$ is the corrosion rate (mm/year), W is the weight loss (mg), D is the density of the sample (g/cm^3), A is the surface area of the sample (cm^2) and T is the duration of the sample is immersed in the solution (h) (Özer *et al.*, 2020).

3. Results and discussion

3.1 Microstructural evaluation

The optical micrographs of the polished cross-sections of the polished samples are given in Figure 2. The micrographs of as-built and HIPed samples indicate that all the materials contain porosities with varying amounts. It was observed that the HIPed samples contain a lesser amount of porosity, which is confirmed by the image analysis results given in Table 4.

Table 4 indicates the amount of open porosity in the samples. The as-built sample has a reasonable porosity value, which is due to the nature of AM. However, as expected, the amount of porosity decreased after HIP and increased after T6 heat treatment. The *H1* sample had the lowest porosity. Therefore, it can be concluded that HIP treatment is an effective method to reduce the porosity in the AM samples. On the other hand, the HIP process does not cause a significant change in the microstructure (Ertuğrul *et al.*, 2020).

The cross-sectional SEM images of the AlSi10Mg samples are given in Figure 3. The as-built microstructure of the AlSi10Mg alloy consists of eutectic Si formed in a very thin cellular form with an α-aluminum matrix. Such a microstructure is the typical result of the very rapid solidification (10^5–10^6 K/s) during the DMLS process (Prashanth and Eckert, 2017; Nakata *et al.*, 2017). Rapid solidification results in insufficient time for the diffusion of Si atoms and the formation of a supersaturated solid solution (Zakay and Aghion, 2019). Due to the nature of the DMLS process, the melt pool boundaries and the heat-affected zone are formed in the structure [Figure 3(a)].

After the HIP process, Si atoms diffuse into nucleation sites, and cellular structure is disrupted. Also, the melt pool boundaries disappear entirely, and the Si particles become coarser [Figure 3(b)]. Si particles grow further and become spherical with subsequent T6 heat treatment [Figure 3(c)–3(e)]. The measured average Si particle sizes are given in Table 5 confirm the findings of the SEM investigation.

3.2 Mechanical properties

Figure 4 shows the hardness values of the samples. The hardness value of the *H0* sample was measured as 85.5 HB. Hardness decreased dramatically after the HIP treatment (*H1* sample/51.1 HB), as can be expected, as there is some solutionizing and grain growth during the high-temperature treatment of the Si-rich Al matrix. For the *H2* sample, the hardness value increased to 110 HB as a result of precipitation hardening. With increasing

Figure 2 Microstructures of the polished AlSi10Mg samples (a) as-built, (b) HIPed, (c) HIP + 4-h aged, (d) HIP + 12-h aged and (e) T6

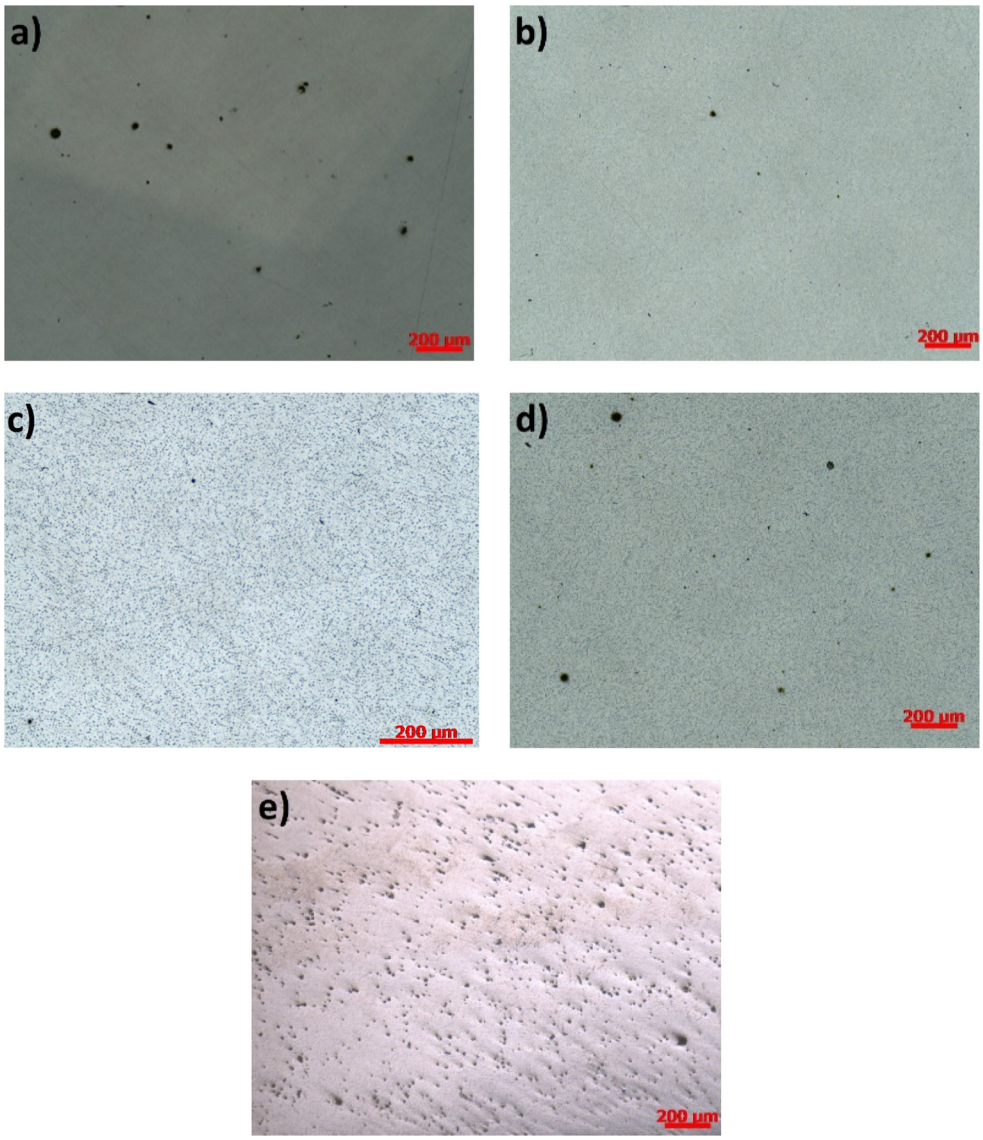

Table 4 Porosity values and standard deviations of the samples

Sample	Porosity – image analysis (%)	Standard deviations (±)
H0	0.203	0.076
H1	0.089	0.021
H2	0.102	0.033
H3	0.110	0.033
T6	0.510	0.009

aging duration, the hardness value decreased (92.1 HB/*H3* sample) due to the excessive coarsening of the Si particles (Table 5) and averaging. Although the hardness of the T6 condition (90.3 HB) was found to be close to the *H3* condition, the hardness value of the *H3* sample was found to be slightly higher, revealing the positive effect of the HIP. These results are following the previous study based on mechanical property investigations with the same system (Ertuğrul *et al.*, 2020).

3.3 Corrosion behaviours

3.3.1 Electrochemical corrosion behaviour

The effects of the HIP and heat treatment conditions on the electrochemical corrosion behaviour of the AlSi10Mg samples were studied using the Tafel polarization method. Figure 5 shows the Tafel polarization curves of the AlSi10Mg samples. Corrosion initiation potential (E_{corr}), corrosion progression rate (I_{corr}), corrosion rate (mm/year) and the polarization resistance (R_p) were obtained from Tafel plots. The T6 sample showed the lowest corrosion potential (−0.7272 V) while the highest corrosion potential value (−0.7941 V) was found in the *H2* sample (Figure 5). In addition, when the corrosion current density values were examined, the T6 sample showed the highest corrosion current density value (0.3884 μA/cm^2). The lowest current density value was found in the *H0* sample (0.1940 μA/cm^2). The current density value of *H1* (0.2958 μA/cm^2) is also relatively low. In *H2* and *H3* samples, current density values were found to be somewhat similar

Figure 3 SEM images of the etched (a) as-produced, (b) HIPed, (c) HIP + 4-h aged, (d) HIP + 12-h aged and (e) T6

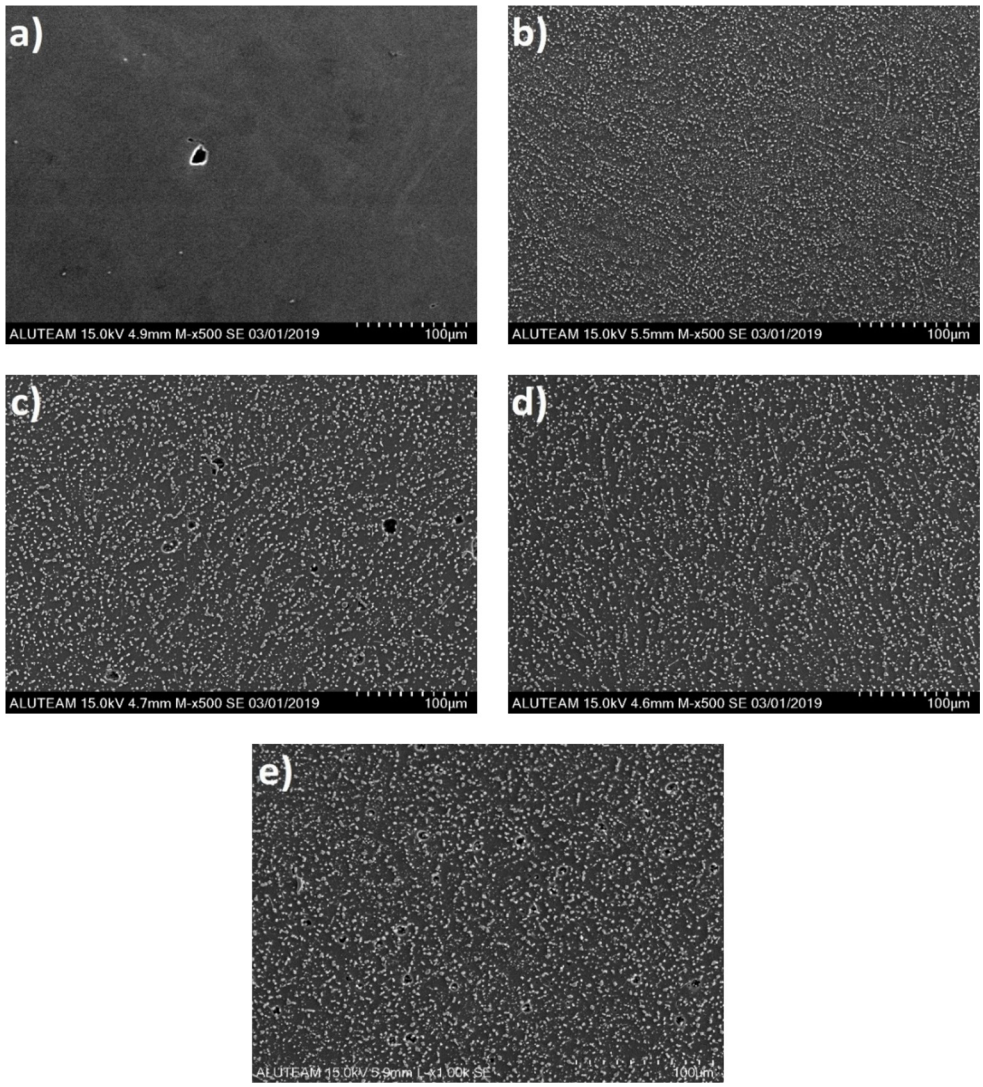

Table 5 Average silicon grain size of the microstructures

Sample	Average silicon grain size (μm)
H0	–
H1	3.26
H2	5.54
H3	6.17
T6	5.87

(0.3538 and 0.3323 μA/cm^2, respectively), which means aging duration does not affect corrosion current density significantly. Polarization resistance (R_p) is inversely proportional to corrosion resistance. In other words, if the polarization resistance is high, the corrosion rate is also low. As seen in Table 6, the *H0* sample showed the highest polarization resistance (37.0 kΩ), which is considerably higher than other samples. In addition, the lowest polarization resistance belongs to the T6 sample (10.3 kΩ). The second highest polarization

Figure 4 Hardness results

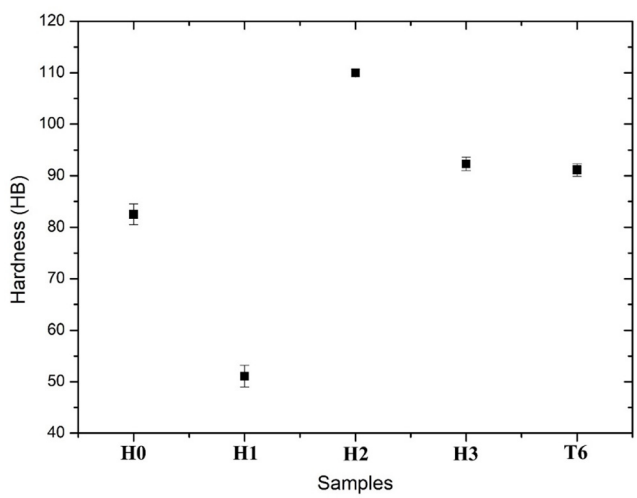

Figure 5 Potentiodynamic polarization curves of the samples

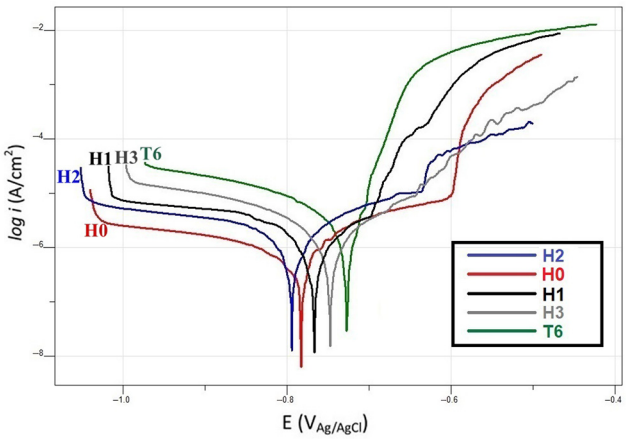

resistance belongs to the *H1* sample (26.6 kΩ), and then to the *H2* sample (24.9 kΩ). The polarization resistance of the *H3* sample is relatively lower (20.8 kΩ).

Corrosion current densities of *H0* and *H1* samples were lower than high-temperature heat-treated samples (*H2*, *H3* and T6). The reason for this is the microstructural alterations. In the *H0* microstructure, silicon particles are distributed through the sample as a very fine network. This very fine distribution of silicon particles has been shown to have a beneficial effect on corrosion by the "small cathode-large anode" mechanism by previous researchers (Girelli *et al.*, 2019b). Rubben *et al.* demonstrated that there is a potential difference between silicon particles and the aluminum matrix they performed on the AM/AlSi10Mg sample using the Scanning Kelvin Probe Force Microscopy (SKPFM) (Rubben *et al.*, 2019). With the heat treatment, the silicon network structure deteriorates, the silicon particles become independent and coarse. As the temperature increases, the size of the silicon particles (cathode) increases (Table 5). Hence, the "small cathode-large anode" mechanism is broken. In this case, the Al matrix, acting as an anode, dissolves faster, and the corrosion rate increases. As a result, solution and T6 heat treatment after HIP treatment increase the corrosion sensitivity of the samples in the saline environment.

Another reason for the decrease in corrosion resistance after high-temperature heat treatment is the formation of intermetallic phases (Fe-containing and Mg_2Si). As the intermetallic phases form a micro galvanic couple with the aluminum matrix, they reduce the corrosion resistance of the samples. Furthermore, the porosity in the microstructure decreases after the HIP process, increasing the corrosion resistance of the samples.

3.3.2 Intergranular corrosion behaviour

Figure 6 shows the variation of weight loss depending on the sample conditions. A sample had the lowest corrosion rate (highest corrosion resistance) in the immersion solution (*H1*), whereas the *H0* sample suffered the fastest corrosion. The T6 sample shows a low corrosion rate. Other samples that were heat-treated after the HIP process (*H2* and *H3*) show moderate corrosion resistance.

The cross-sectional images of the samples after the immersion in the intergranular test solution for 24 h are given in Figure 7. As seen in Figure 7, the immersion corrosion behaviour is different from electrochemical corrosion behaviour. Corrosion damage is seen as a penetrating attack in the sample with *H0*. This is related to the microstructure formed after the stress relief heat treatment applied to the as-built structure. In such a microstructure, the cellular Si network formed in the as-built microstructure is disrupted and becomes discontinuous. However, melt pool boundaries do not disappear completely. IGC damage in such a microstructure proceeds deeper in a lightning-like structure. The cause of this corrosion damage is the selective attack of the material along the melt pool boundaries. That is, the *H0* sample is locally subjected to a selective corrosion attack.

The HIPed sample was hardly corroded [Figure 7(b)]. This situation is related to the porosity in the microstructure. After the HIP procedure, the micro porosities in the structure decrease considerably. DMLS as-built samples have porosity due to the nature of the production method, making the samples susceptible to micro-cracks (Subrahmanyam *et al.*, 2020; Cabrini *et al.*, 2019; Aboulkhair *et al.*, 2014). These cracks preferentially form starting points for corrosion damage in corrosive

Figure 6 Variation of the weight loss depending on different sample conditions

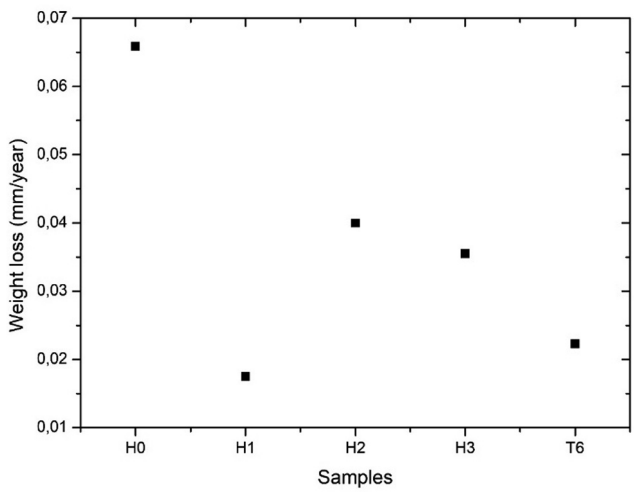

Table 6 Results of the potentiodynamic polarization tests

Samples	E_{corr} (V)	I_{corr} (μA/cm^2)	Corrosion rate (mm/year)	Polarization resistance (kΩ)
H0	−0.7823	0.1940	0.002192	37.0
H1	−0.7670	0.2958	0.003168	26.6
H2	−0.7941	0.3538	0.003998	24.9
H3	−0.7472	0.3323	0.003755	20.8
T6	−0.7272	0.3884	0.004390	10.3

Figure 7 Cross-sectional images of the samples after the IGC test, (a) as-built, (b) HIPed, (c) HIP + 4-h aged, (d) HIP + 12-h aged and (e) T6

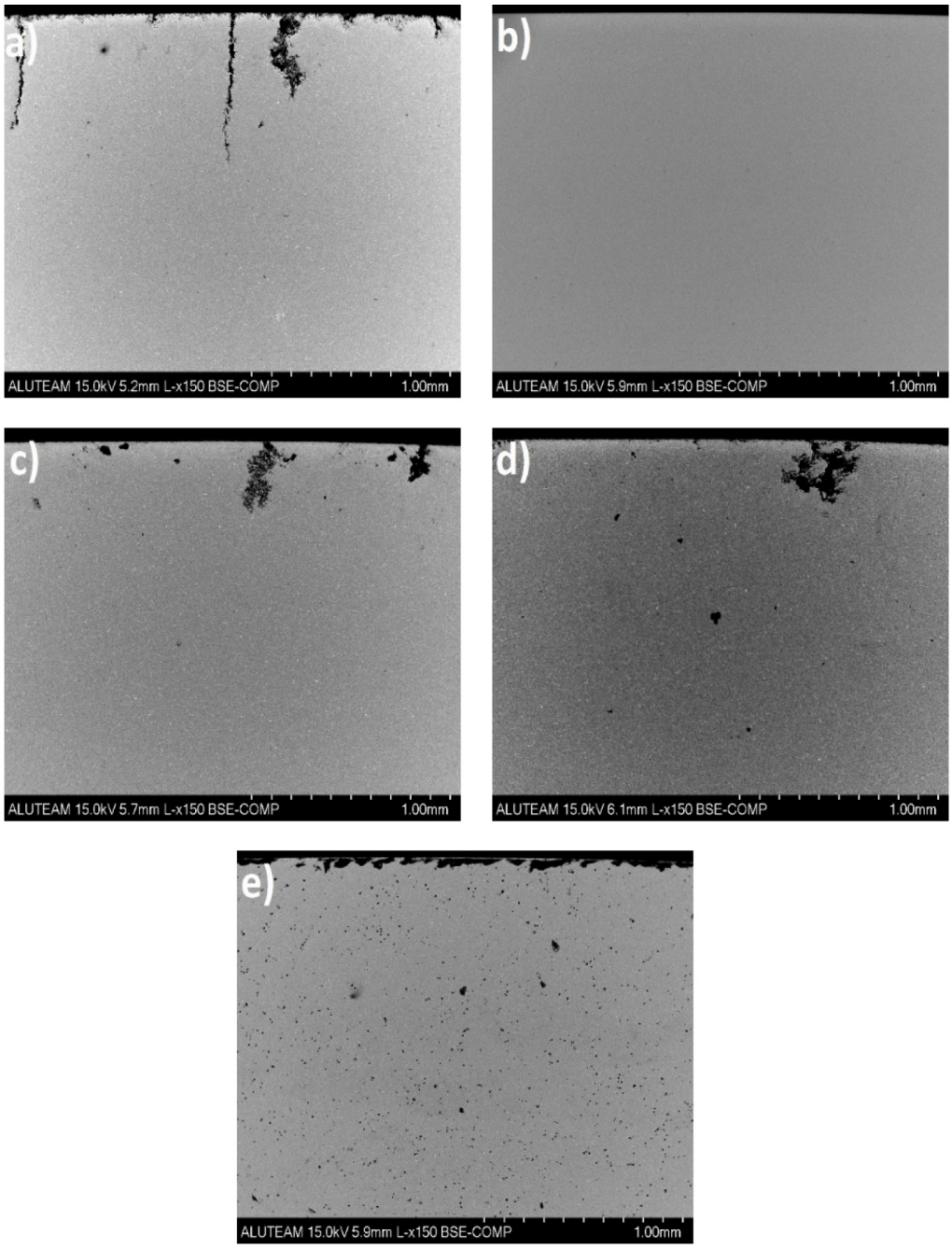

environments (Cabrini *et al.*, 2016a). It can be concluded that the HIP process reduces the risk of cracking, and the samples become more resistant to corrosion.

After high-temperature heat treatment, a different mechanism emerges. The melt pool boundaries in the microstructure disappear completely, the cellular silicon network is broken, and the silicon particle become coarse [Figure 3(c)–3(e)]. In this case, the corrosion behaviour of the material also changes. The preferential corrosion progression seen in the *H0* sample is not seen in these samples. Corrosion damage is mostly observed in the form of pits in samples that have been heat-treated at high temperatures [Figure 7(c)–7(e)].

The IGC behaviour of the material is different from electrochemical corrosion behaviour. "Small cathode-large anode" mechanism is effective in electrochemical corrosion. As heat treatments performed at high temperatures disrupt this mechanism (Si particles become coarse), the alloy shows higher corrosion resistance in the as-built state.

In ICG, the corrosion damage proceeds along the grain boundaries. Therefore, in the as-built case where grain boundaries exist, the alloy suffers more damage. High-temperature heat treatments homogenize the microstructure. The cellular Si network structure deteriorates, and grain boundaries are lost. With the

disappearance of grain boundaries, corrosion cannot progress along the grain boundaries, and instead, it appears as pits (Figure 7).

The *H1* (HIPed) sample showed the lowest corrosion sensitivity. Porosities in the microstructure preferentially form the starting points of corrosion in the IGC solution. Therefore, after the HIP process, the porosity decreases considerably, decreasing the corrosion initiation and progress rate.

4. Conclusions

The main conclusions deduced from this work are as follows:

- AlSi10Mg alloy samples produced with DMLS contained micro porosities due to the nature of the production method. It was that the HIP process significantly reduced these micro porosities.
- DMLS/AlSi10Mg microstructure consisted of a very fine cellular eutectic Si and aluminum matrix. The melt pool boundaries were apparent in the microstructure. After the HIP process, this microstructure was degraded with the effect of temperature, and the Si particles became independent and coarse. T6 heat treatment performed after the HIP process made these Si particles even coarser.
- The HIP process reduced the hardness as it altered the as-built microstructure. However, the short T6 heat treatment performed after the HIP process increased the hardness by precipitation hardening. However, longer T6 heat treatment caused overaging and reduced hardness.
- The *H0* sample showed the lowest corrosion sensitivity in a 3.5% NaCl solution. This was due to the "small cathode-large anode" mechanism in the *H0* microstructure. Relatively low corrosion sensitivity was seen after the HIPed process. As the HIPed process reduces the porosities in the microstructure of the alloy, it has a beneficial effect on corrosion resistance. However, as the T6 heat treatment performed after HIPed coarse the Si particles and disrupts the "small cathode-large anode" mechanism, its corrosion resistance decreases.
- The IGC behaviour of AlSi10Mg alloy was completely different. The *H0* sample showed the lowest corrosion resistance in IGC. This was because of the melt pool boundaries that exist in the microstructure. IGC progresses along these boundaries and damages the material. The IGC resistance of the alloy increases as the HIP process and subsequent heat treatments remove the grain boundaries in the microstructure and homogenize the microstructure. In addition, as HIPed significantly reduces the porosity in the microstructure, the IGC strength of the alloy increases.

References

Aboulkhair, N.T., Everitt, N.M., Ashcroft, I. and Tuck, C. (2014), "Reducing porosity in AlSi10Mg parts processed by selective laser melting", *Additive Manufacturing*, Vols 1/4 No. 4, pp. 77-86.

Aboulkhair, N.T., Maskery, I., Tuck, C., Ashcroft, I. and Everitt, N.M. (2016), "The microstructure and mechanical properties of selectively laser melted AlSi10Mg: the effect of a conventional T6-like heat treatment", *Materials Science and Engineering A*, Vol. 667, pp. 130-146.

Cabrini, M., Lorenzi, S., Pastore, T., Pellegrini, S., Ambrosio, E.P., Calignano, F., Manfredi, D., Pavese, M. and Fino, P. (2016a), "Effect of heat treatment on corrosion resistance of DMLS AlSi10Mg alloy", *Electrochimica Acta*, Vol. 206, pp. 346-355.

Cabrini, M., Lorenzi, S., Pastore, T., Pellegrini, S., Manfredi, D., Fino, P., Biamino, S. and Badini, C. (2016b), "Evaluation of corrosion resistance of al–10Si–Mg alloy obtained by means of direct metal laser sintering", *Journal of Materials Processing Technology*, Vol. 231, pp. 326-335.

Cabrini, M., Lorenzi, S., Pastore, T., Pellegrini, S., Pavese, M., Fino, P., Ambrosio, E.P., Calignano, F. and Manfredi, D. (2016c), "Corrosion resistance of direct metal laser sintering AlSiMg alloy", *Surface and Interface Analysis*, Vol. 48 No. 8, pp. 818-826.

Cabrini, M., Calignano, F., Fino, P., Lorenzi, S., Lorusso, M., Manfredi, D., Testa, C. and Pastore, T. (2018), "Corrosion behavior of heat-treated AlSi10Mg manufactured by laser powder bed fusion", *Mater*, Vol. 11 No. 7, pp. 1-14.

Cabrini, M., Lorenzi, S., Pastore, T., Testa, C., Manfredi, D., Larusso, M., Calignano, F., Pavese, M. and Andreatta, F. (2019), "Corrosion behavior of AlSi10Mg alloy produced by laser powder bed fusion under chloride exposure", *Corrosion Science*, Vol. 152, pp. 101-108.

Ceschini, L., Morri, A. and Sambogna, G. (2008), "The effect of hot isostatic pressing on the fatigue behaviour of sand-cast A356-T6 and A204-T6 aluminum alloys", *Journal of Materials Processing Technology*, Vol. 204 Nos 1/3, pp. 231-238.

Delahaye, J., Tchoufang Tchuindjang, J., Lecomte-Beckers, J., Rigo, O., Habraken, A.M. and Mertens, A. (2019), "Influence of Si precipitates on fracture mechanisms of AlSi10Mg parts processed by selective laser melting", *Acta Materialia*, Vol. 175, pp. 160-170.

EOS (2021), "EOS aluminum AlSi10Mg material data sheet", available at: www.eos.info/03_system-related-assets/material-related-contents/metal-materials-and-examples/metal-material-datasheet/aluminium/material_datasheet_eos_aluminium-alsi10mg_en_web.pdf

Ertuğrul, O., Öter, Z.Ç., Yılmaz, M.S., Şahin, E., Coşkun, M., Tarakçı, G. and Koç, E. (2020), "Effect of HIP process and subsequent heat treatment on microstructure and mechanical properties of direct metal laser sintered AlSi10Mg alloy", *Rapid Prototyping Journal*, Vol. 26 No. 8, pp. 1421-1434.

Girelli, L., Giovagnoli, M., Tocci, M., Pola, A., Fortini, A., Merlin, M. and La Vecchia, G.M. (2019a), "Evaluation of the impact behaviour of AlSi10Mg alloy produced using laser additive manufacturing", *Materials Science and Engineering: A*, Vol. 748, pp. 38-51.

Girelli, L., Tocci, M., Conte, M., Giovanardi, R., Veronesi, P., Gelfi, M. and Pola, A. (2019b), "Effect of the T6 heat treatment on corrosion behavior of additive manufactured and gravity cast AlSi10Mg alloy", *Materials and Corrosion*, Vol. 70 No. 10, pp. 1808-1816.

Girelli, L., Tocci, M., Gelfi, M. and Pola, A. (2019c), "Study of heat treatment parameters for additively manufactured AlSi10Mg in comparison with corresponding cast alloy", *Materials Science and Engineering: A*, Vol. 739, pp. 317-328.

Gu, X.H., Zhang, J.X., Fan, X.L. and Zhang, L.C. (2019), "Corrosion behavior of selective laser melted AlSi10Mg alloy in NaCl solution and its dependence on heat treatment", *Acta Metallurgica Sinica (English Letters)*, Vol. 33 No. 3, pp. 327-337.

Herzog, D., Seyda, V., Wycisk, E. and Emmelmann, C. (2016), "Additive manufacturing of metals", *Acta Materialia*, Vol. 117, pp. 371-392.

Iturrioz, A., Gil, E., Petite, M.M., Garciandia, F., Mancisidor, A.M. and San Sebastian, M. (2018), "Selective laser melting of AlSi10Mg alloy: influence of heat treatment condition on mechanical properties and microstructure", *Welding in the World*, Vol. 62 No. 4, pp. 885-892.

Kempen, K., Thijs, L., Van Humbeeck, J. and Kruth, J.P. (2012), "Mechanical properties of AlSi10Mg produced by selective laser melting", *Physics Procedia*, Vol. 39, pp. 439-446.

Krishnan, M., Atzeni, E., Ganali, R., Galignano, F., Manfredi, D. and Ambrosio, E.P. (2013), "On the effect of process parameters on properties of AlSi10Mg parts produced by DMLS", *Rapid Prototyping Journal*, Vol. 20 No. 6, pp. 449-458.

Lee, M.H., Kim, J.J., Kim, K.H., Kim, N.J., Lee, S. and Lee, E. W. (2003), "Effect of HIPping on high-cycle fatigue properties of investment cast A356 aluminum alloys", *Materials Science and Engineering: A*, Vol. 340 Nos 1/2, pp. 123-129.

Li, W., Li, S., Liu, J., Zhang, A., Zhou, Y., Wei, Q., Yan, C. and Shi, Y. (2016), "Effect of heat treatment on AlSi10Mg alloy fabricated by selective laser melting: microstructure evolution, mechanical properties, and fracture mechanism", *Materials Science and Engineering: A*, Vol. 663, pp. 116-125.

Maamoun, A.H., Elbestawi, M., Dosbaeva, G.K. and Veldhuis, S.C. (2018), "Thermal post-processing of AlSi10Mg parts produced by selective laser melting using recycled powder", *Additive Manufacturing*, Vol. 21, pp. 234-247.

Nakata, N., Kodaira, H., Sekizawa, K., Suzuki, A. and Kobashi, M. (2017), "Change in microstructure of selectively laser melted AlSi10Mg alloy with heat treatments", *Materials Science and Engineering: A*, Vol. 704, pp. 218-228.

Ni, M., Liu, S., Chen, C., Li, R., Zhang, X. and Zhou, K. (2019), "Effect of heat treatment on the microstructural evolution of a precipitation-hardened superalloy produced by selective laser melting", *Materials Science and Engineering: A*, Vol. 748, pp. 275-285.

Olakanmi, E., Cochrane, K. and Dalgarno, K. (2015), "A review on selective laşer sintering/melting (SLS/SLM) of aluminium alloy powders: processing, microstructure, and properties", *Progress in Materials Science*, Vol. 74, pp. 401-477.

Özer, G., Tarakci, G., Yilmaz, M.S., Öter, Z.Ç., Sürmen, Ö., Akça, Y., Coşkun, M. and Koç, E. (2020), "Investigation of the effects of different heat treatment parameters on the corrosion and mechanical properties of the AlSi10Mg alloy produced with direct metal laser sintering", *Materials and Corrosion*, Vol. 71 No. 3, pp. 365-373.

Prashanth, K. and Eckert, J. (2017), "Formation of metastable cellular microstructures in selective laser melted alloys", *Journal of Alloys and Compounds*, Vol. 707, pp. 27-34.

Rafieazada, M., Mohammadi, M. and Nasiri, A.M. (2019), "On microstructure and early stage corrosion performance of heat treated direct metal laser sintered AlSi10Mg", *Additive Manufacturing*, Vol. 28, pp. 107-119.

Ran, G., Zhou, J. and Wang, Q.G. (2006), "The effect of hot isostatic pressing on the microstructure and tensile properties of an unmodified A356-T6 cast aluminum alloy", *Journal of Alloys and Compounds*, Vol. 421 Nos 1/2, pp. 80-86.

Read, N., Wang, W., Essa, K. and Attallah, M.M. (2015), "Selective laser melting of AlSi10Mg alloy: process optimisation and mechanical properties development", *Materials and Design (1980-2015)*, Vol. 65, pp. 417-424.

Rubben, T., Revilla, R.I. and Graeve, I.D. (2019), "Influence of heat treatments on the corrosion mechanism of additive manufactured AlSi10Mg", *Corrosion Science*, Vol. 147, pp. 406-415.

Salman, O.O., Gammer, C., Chaubey, A.K., Eckert, J. and Scudino, S. (2019), "Effect of heat treatment on microstructure and mechanical properties of 316l steel synthesized by selective laser melting", *Materials Science and Engineering: A*, Vol. 748, pp. 205-212.

Schneller, W., Leitner, M., Springer, S., Grün, F. and Taschauer, M. (2019), "Effect of HIP treatment on microstructure and fatigue strength of selectively laser melted AlSi10Mg", *Journal of Manufacturing and Materials Processing*, Vol. 3 No. 1, p. 16.

Sing, S., An, J., Yeong, W. and Wiria, F. (2016), "Laser and electron-beam powder-bed additive manufacturing of metallic implants: a review on processes, materials and designs", *Journal of Orthopaedic Research*, Vol. 34 No. 3, pp. 369-385.

Subrahmanyam, A.P.S.V.R., Prasad, K.S. and Rao, P.S. (2020), "A review on mechanical and corrosion behaviour of DMLS materials", *Engineering Science and Technology*, Vol. 1 No. 2, pp. 62-83.

Vrancken, B., Thijs, L., Kruth, J.P. and Van Humbeeck, J. (2012), "Heat treatment of Ti6Al4V produced by selevtive laser melting: microstructure, and mechanical properties", *Journal of Alloys and Compounds*, Vol. 541 No. 15, pp. 177-185.

Wang, L.F., Sun, J., Yu, X.L., Shi, Y., Zhu, X.G., Cheng, L.Y., Liang, H.H., Yan, B. and Guo, L.J. (2018), "Enhancement in mechanical properties of selectively laser-melted AlSi10Mg aluminum alloys by T6-like heat treatment", *Materials Science and Engineering: A*, Vol. 734, pp. 299-310.

Wang, X., Xu, S., Zhou, S., Xu, W., Leary, M., Choong, P., Qian, M., Brandt, M. and Xie, Y. (2016), "Topological design and additive manufacturing of porous metals for bone scaffolds and orthopaedic implants: a review", *Biomaterials*, Vol. 83, pp. 127-141.

Zakay, A. and Aghion, E. (2019), "Effect of post-heat treatment on the corrosion behavior of AlSi10Mg alloy produced by additive manufacturing", *JOM*, Vol. 71 No. 3, pp. 1150-1157.

Zhou, L., Mehta, A., Sculz, E., McWilliams, B., Cho, K. and Shon, Y. (2018), "Microstructure, precipitates and hardness of selectively laser melted AlSi10Mg alloy before and after heat treatment", *Materials Characterization*, Vol. 143, pp. 5-17.

Corresponding author

Mustafa Safa Yılmaz can be contacted at: m.safayilmaz@gmail.com